Toroidal and Slab ETG Dominance in the Linear Spectrum of JET-ILW Pedestals

Jason Parisi[1,2]

with

Felix Parra[1], Colin Roach[2], Carine Giroud[3], William Dorland[1,4], David Hatch[5], Nobuyuki Aiba[6], Michael Barnes[1], Plamen Ivanov[1]

University of Oxford [1], CCFE [2], JET [3], University of Maryland [4], UT Austin [5], Rokkasho Fusion Institute [6]

European Fusion Theory Conference

October 10 2019

The pedestal is a ubiquitous feature of H-mode plasmas.

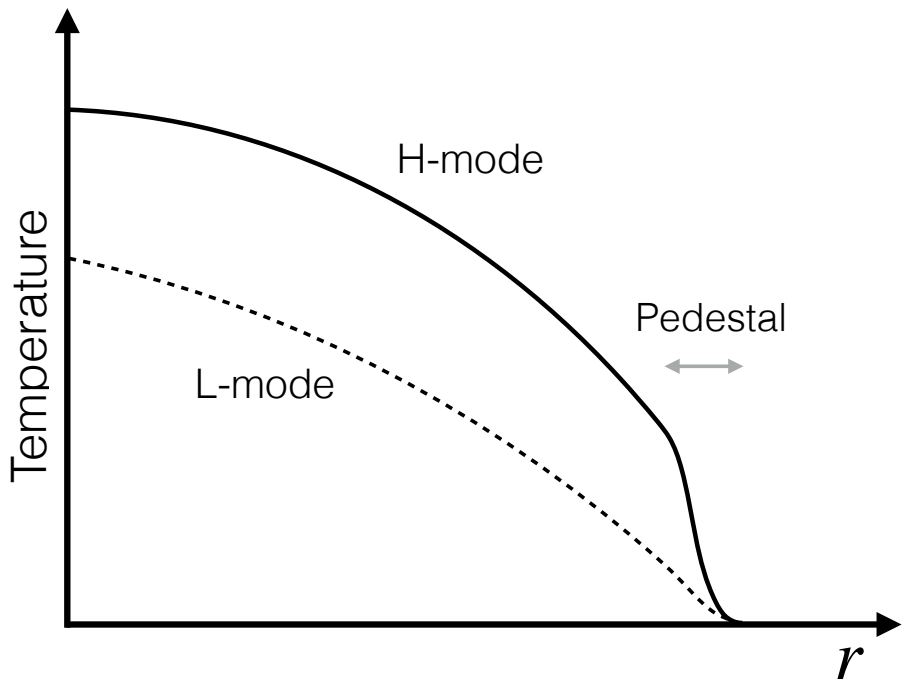

Figure: Typical temperature profiles for L-mode and H-mode discharges.

- Pedestal is an edge region of increased equilibrium gradients and reduced turbulent fluxes.
- Appears once heating exceeds a threshold value.
- Discovered on ASDEX [Wagner, 1982], but physics for its formation still not clear.

- Purpose of this work is to understand microinstabilities in the pedestal.

Pedestal extends around $\overline{\psi} = 0.9 - 1.0$, where $\overline{\psi} = \psi/\psi(\mathrm{LCFS})$, and ψ is the poloidal flux.

Figure: Surfaces of constant $\overline{\psi}$ for a JET-ILW discharge 92174. Pedestal region is highlighted.

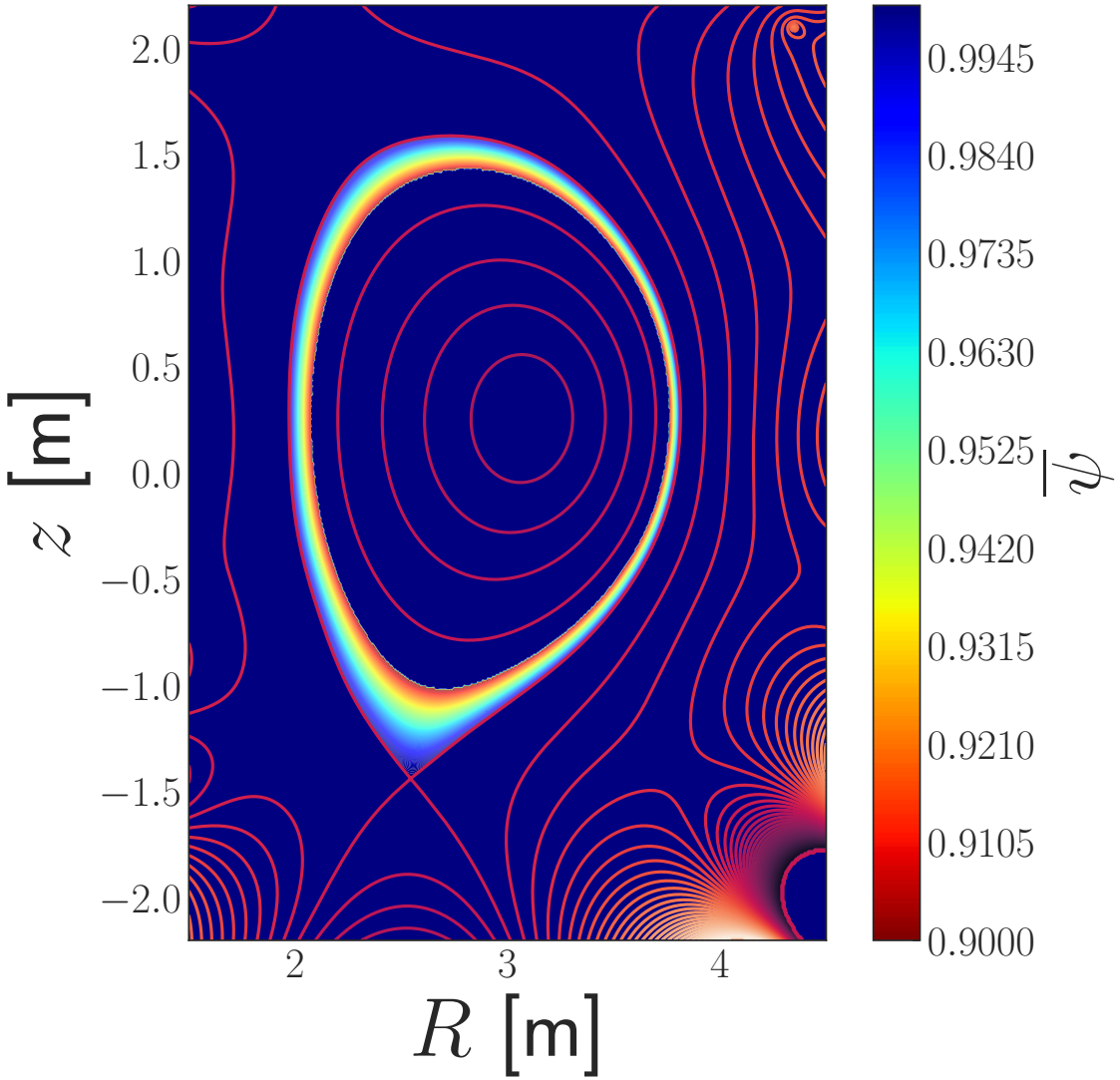

Pedestal equilibrium gradients are much bigger than in the core.

- $R/L_{Te} \approx 50 - 400$, $R/L_{Ti} \approx 30 - 100$. In core, $R/L_{Ts} \approx 5 - 10$. Here R is the major radius, $L_{Ts} \equiv -(\nabla \ln T_s)^{-1}$.
  $\Rightarrow$ dramatic consequences for ETG and ITG(?) stability!
- Measured T_i flatter than T_e in pedestal shots we examined, although $T_i = T_e$ case also investigated.
- In this talk, focus on inter-ELM period of JET shot 91274, C2D4 gas injection discharge.

Figure: Temperature and density gradients, JET-ILW shot 92174. Crosses mark gyrokinetic simulation location.

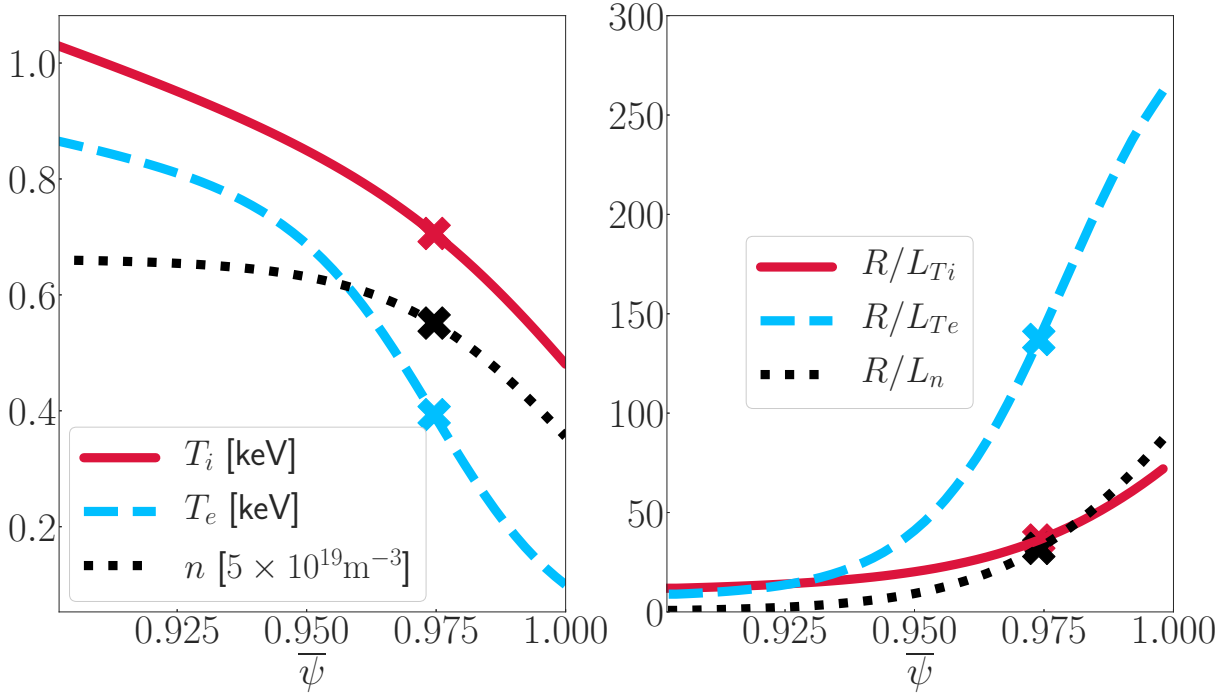

- Use $\{x, y, \theta\}$ real space coordinates: x radial, y field line label.
- Perpendicular perturbation wavenumber, $k_\perp$, with magnetic shear $\hat{s}$,

$$k_\perp \approx \sqrt{k_x^2 + k_y^2} \approx k_y \sqrt{(\hat{s}\theta)^2 + 1}, \tag{1}$$

where $k_x = k_{x0} - k_y \hat{s}\theta$ is an effective radial wavenumber.

- Frequencies, $\omega_{\kappa,s} \equiv \mathbf{k}_\perp \cdot \mathbf{v}_{Ms}$, $\omega_{*e} = \mathbf{v}_E^t \cdot \nabla \ln(n) \frac{T_e}{e\phi^t} = \frac{k_y v_{te} \rho_e}{L_n}$,
where $\mathbf{v}_{Ms} = \frac{1}{\Omega_s}(\hat{\mathbf{b}} \times \nabla \ln \mathbf{B})(v_\parallel^2 + v_\perp^2/2)$ is the magnetic drift.

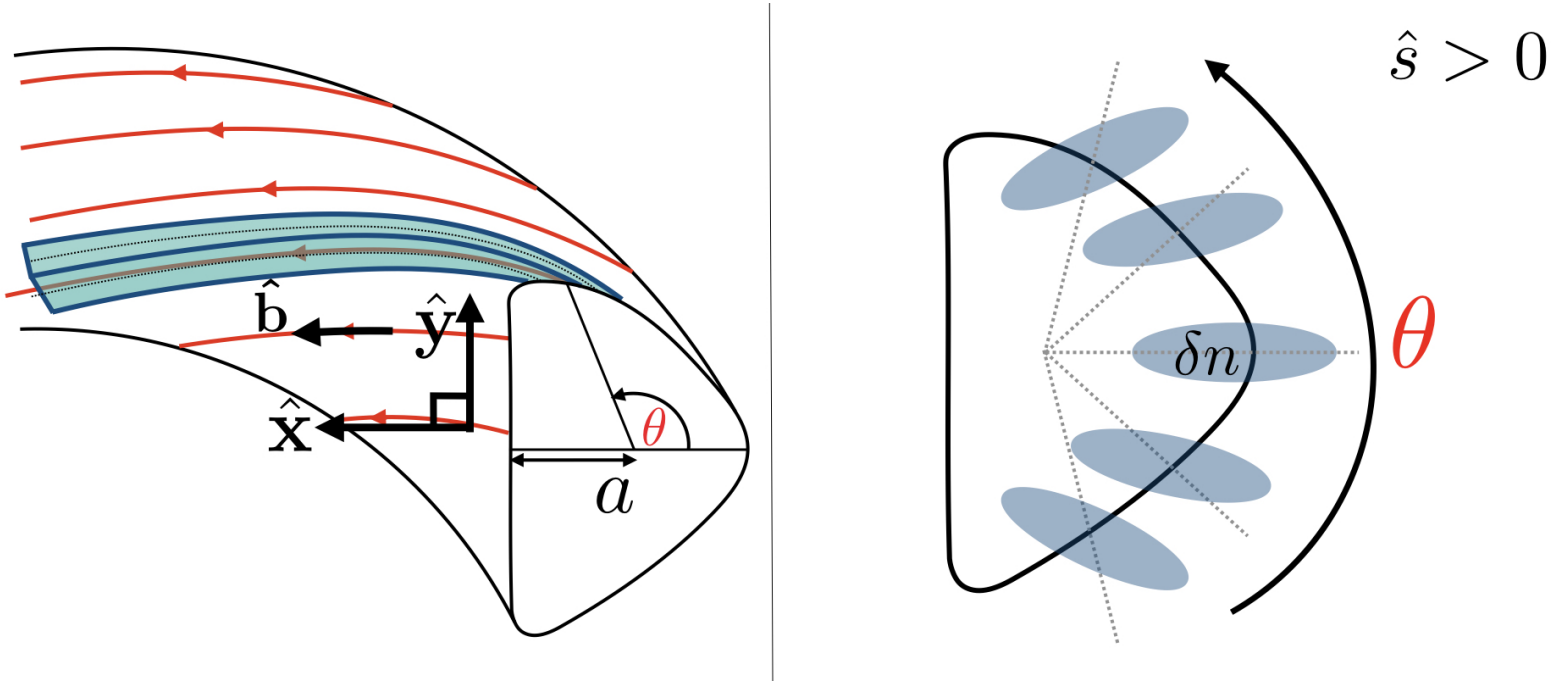

Figure 4: Left: coordinates. Right: magnetic shear acting on perturbation.

Toroidal ETG can be more virulent than expected.

- **Naive** relative size of toroidal and slab drives shows slab dominates, since $k_\parallel$ can become large with k_y for slab,

$$\text{toroidal}: \frac{\omega_{*e}\eta_e}{\omega_{\kappa,e}} \sim \frac{R}{L_{Te}} \gg 1, \quad \text{slab}: \frac{\omega_{*e}\eta_e}{k_\parallel v_{te}} \sim \frac{k_y}{k_\parallel}\frac{\rho_e}{L_{Te}}. \tag{2}$$

  where $\eta_s \equiv L_n/L_{Ts}$.

- **More careful** analysis for toroidal branch shows

$$\text{toroidal}: \frac{\omega_{*e}\eta_e}{\omega_{\kappa,e}} \sim \frac{k_y}{k_\perp}\frac{R}{L_{Te}} \sim \frac{1}{\sqrt{(\hat{s}\theta)^2+1}}\frac{R}{L_{Te}}. \tag{3}$$

  Important! (a): ω_{*e} independent of k_x (b): $k_\perp$ increases along θ due to $\hat{s}$.

- In core, $R/L_{Te} \sim 1$, so dominant toroidal mode at $\theta \sim 0$.
- In pedestal, since $R/L_{Te} \gg 1$, could allow $\hat{s}\theta \gg 1$, and thus toroidal ETG driven at $\hat{s}\theta \gg 1$ ($\rightarrow k_x \gg k_y$), competes with slab ETG.
- Can a toroidal mode find a sufficiently large θ such that it can become large? **We will show it can!**

In pedestal can strongly drive toroidal ETG at $k_y\rho_i \sim 1$ but $k_x\rho_e \sim 1$.

- Figure 5 shows strong toroidal ETG drive at,

$$\frac{\omega_{*e}\eta_e}{\omega_{\kappa,e}} \sim \frac{1}{\sqrt{(\hat{s}\theta)^2+1}}\frac{R}{L_{Te}} \sim 1. \qquad (4)$$

- Thus strong toroidal ETG at

$$\hat{s}\theta \sim \frac{R}{L_{Te}}. \qquad (5)$$

- FLR considerations require $\boxed{k_\perp\rho_e \sim 1}$, FLR damps $k_\perp\rho_e \gg 1$.
- Thus for $\hat{s}\theta \sim R/L_{Te}$,

$$k_\perp\rho_e \sim k_x\rho_e \sim k_y\rho_e\hat{s}\theta \sim 1 \qquad (6)$$

$$\Rightarrow \; k_y\rho_i \sim \sqrt{\frac{m_iT_i}{m_eT_e}}\frac{L_{Te}}{R} \sim 1 \qquad (7)$$

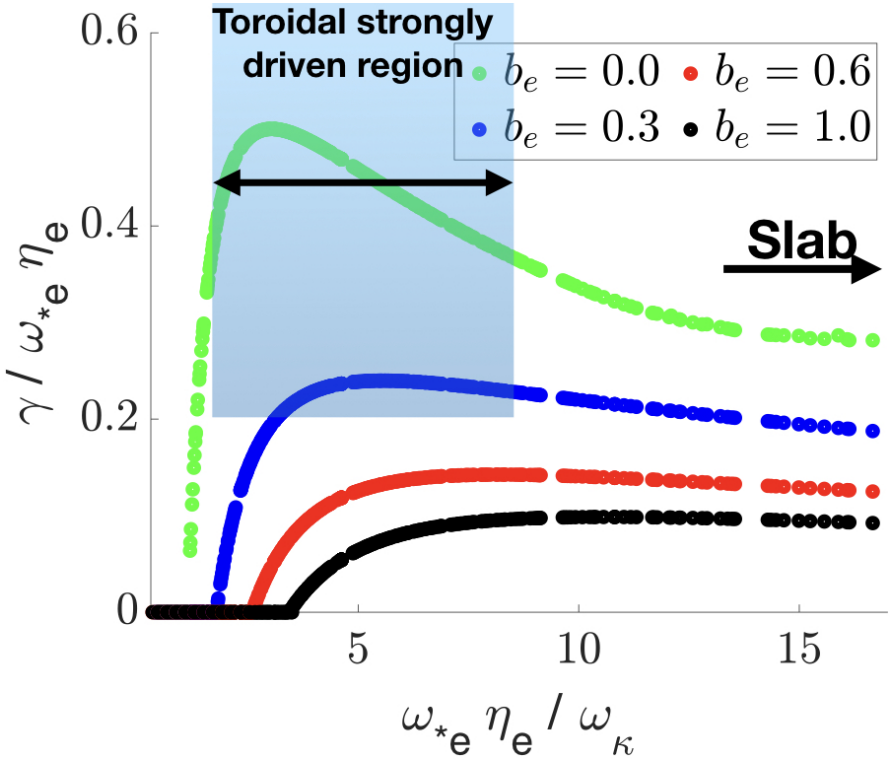

Figure 5: Growth rates for toroidal ETG dispersion relation for $\boxed{b_e = (k_\perp\rho_e)^2/2}$.

- Can show slab ETG driven at $k_y\rho_i \sim \sqrt{m_iT_i/m_eT_e}L_{Te}/R \sim 1$, but $k_x\rho_i \sim 1$.

ITG quenched in JET pedestal simulations, ETG dominant.

- Similarly can show toroidal ITG strongly driven at $k_y\rho_i \sim L_{Ti}/R \ll 1$, $k_x\rho_i \sim 1$.
- Electrostatic ITG has been named as a dominant transport channel in JET pedestals [Hatch 2016, 2017].
- **However**, in JET-ILW pedestals, often true that $R/L_{Te} > R/L_{Ti}, \quad \eta_e > \eta_i$, might expect ITG to be weak.
- In our JET-ILW simulations, since $\eta_i \sim 1$, slab ITG weak or absent, and R/L_{Ti} too small for strong toroidal ITG.

  $\Rightarrow$ ITG weak/absent in our pedestal simulations (shown later).

With $R/L_{Ts} \gg 1$, new temperature gradient instability landscape.
(assuming equal ion and electron pressure profiles).

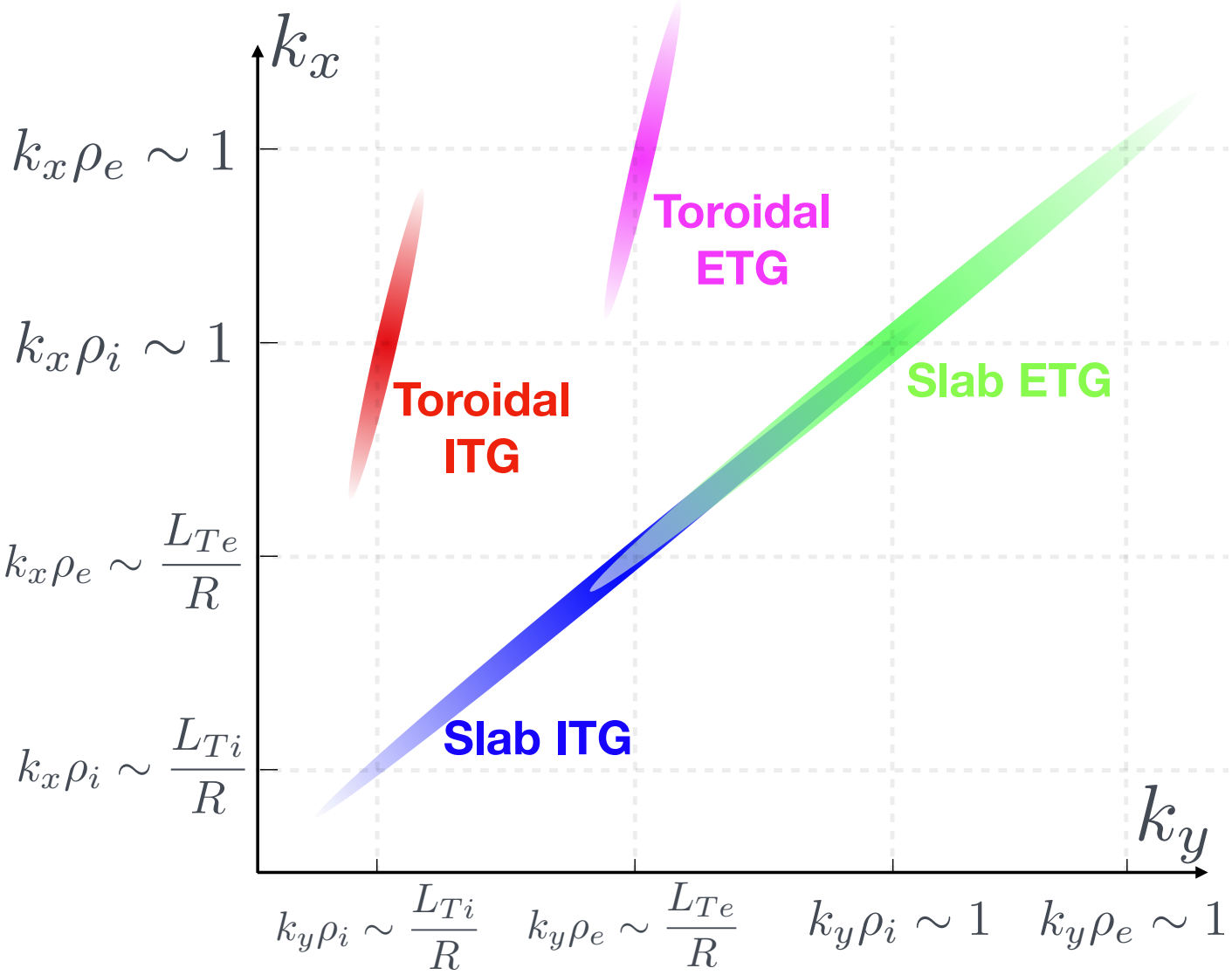

Figure 6: Slab and toroidal temperature gradient instabilities when $R/L_{Ts} \gg 1$. Color indicates locations of instability.

- Linear electrostatic gyrokinetic simulations of JET pedestals to investigate microinstability physics using GS2.
- Simulations carried out at location marked by crosses.
- $\mathbf{E} \times \mathbf{B}$ shear linearly suppress all electromagnetic modes, motivating electrostatic study.

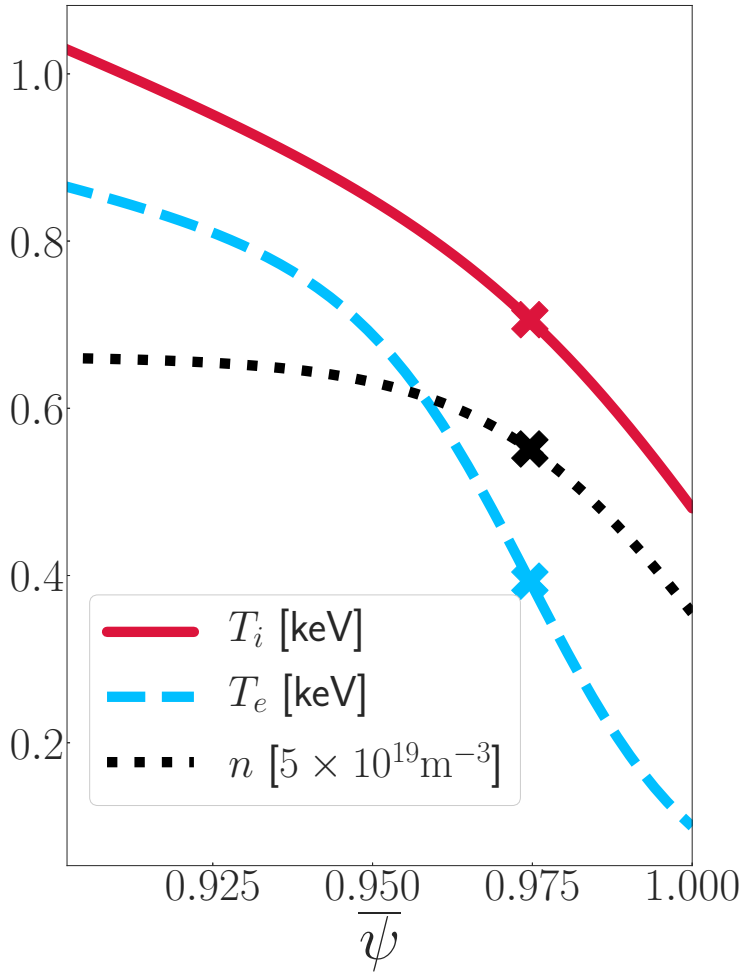

Figure 7: Simulation location for JET shot 92174.

Kinetic ballooning modes (KBMs) sheared by $\mathbf{E} \times \mathbf{B}$ shear $\Rightarrow$ do only electrostatic study

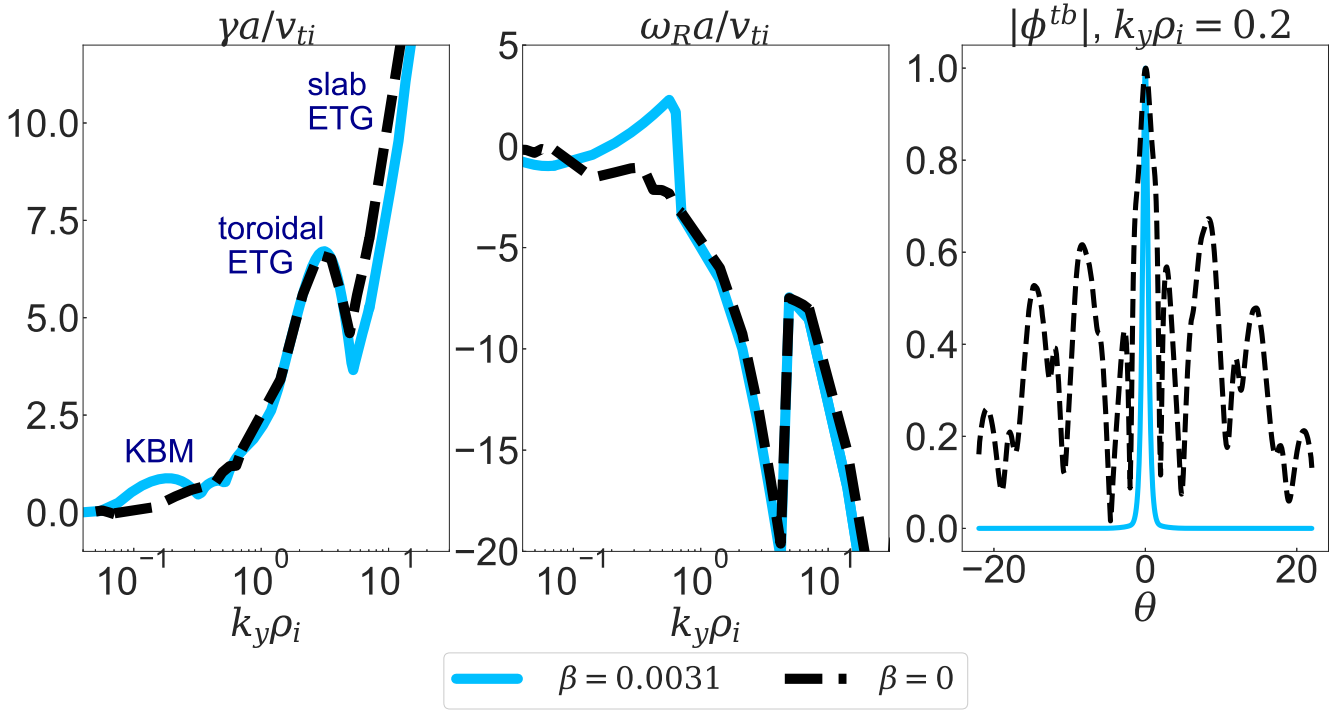

Figure 8: GS2 growth rates (left), real frequencies (middle), eigenmodes (right) for electromagnetic and electrostatic pedestals.

- Most modes propagate in electron diamagnetic direction.
- $\mathbf{E} \times \mathbf{B}$ shear suppresses KBM, rest of spectrum $\approx$ electrostatic.
- Unsurprising that flow shear damps KBM since very localized in θ_0 (radially extended).

  $\Rightarrow$ **undergo electrostatic study.**

$\mathbf{E} \times \mathbf{B}$ shear suppresses KBMs, ITG, but not ETG.

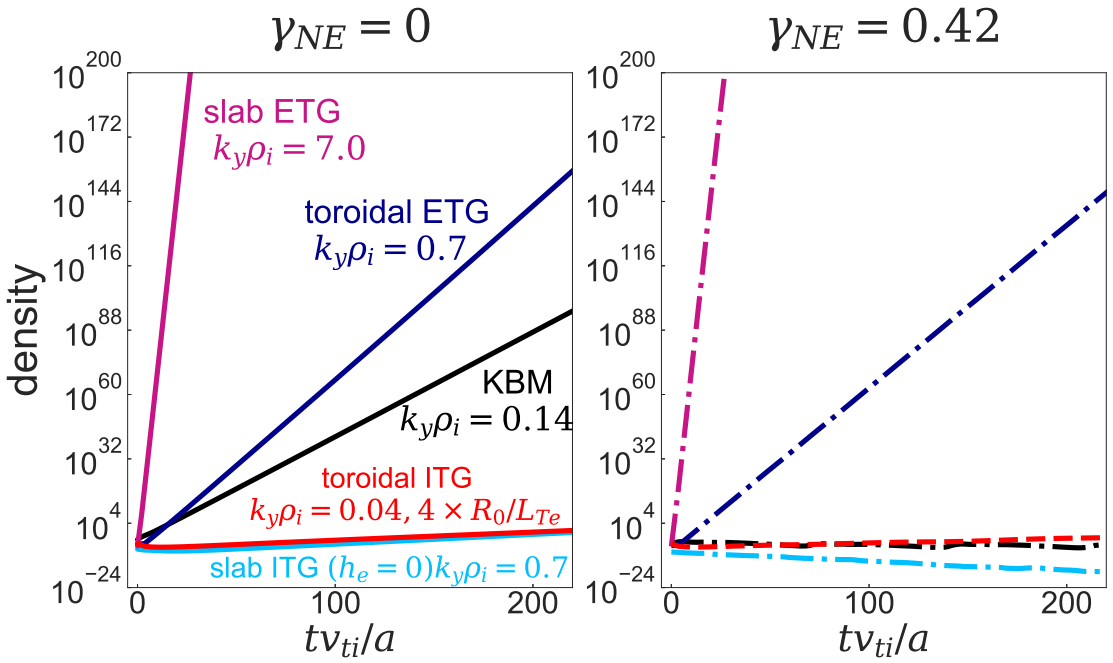

Figure 9: Effect of $\mathbf{E} \times \mathbf{B}$ shear on different modes.

- KBMs and high $k_y\rho_i$ ITG **easily suppressed** by $\mathbf{E} \times \mathbf{B}$ shear: slab ITG is easily sheared, toroidal ITG harder to shear.

- $k_y\rho_i \sim L_{Ti}/R$ toroidal ITG growth rate reduced substantially by $\mathbf{E} \times \mathbf{B}$ shear, but often still unstable.
- ETG **very resistant** to $\mathbf{E} \times \mathbf{B}$ shear.

Gyrokinetic Results ⟩ $1 \lesssim k_y\rho_i \lesssim 5$ Spectra

Modes insensitive to R/L_{Ti}, very sensitive to R/L_{Te}.

- Top: $R/L_{Te}, R/L_n$ scans. **Toroidal and slab modes have very strong $\mathbf{R/L_{Te}}$ dependence.** Slab modes also depend on R/L_n.
- Bottom: R/L_{Ti} scans. **Toroidal ETG modes completely insensitive to R/L_{Ti}. Even for $R/L_{Ti} \gg R/L_{Te}$, spectrum invariant.** **Slab modes some $\mathbf{R/L_{Ti}}$ sensitivity.**

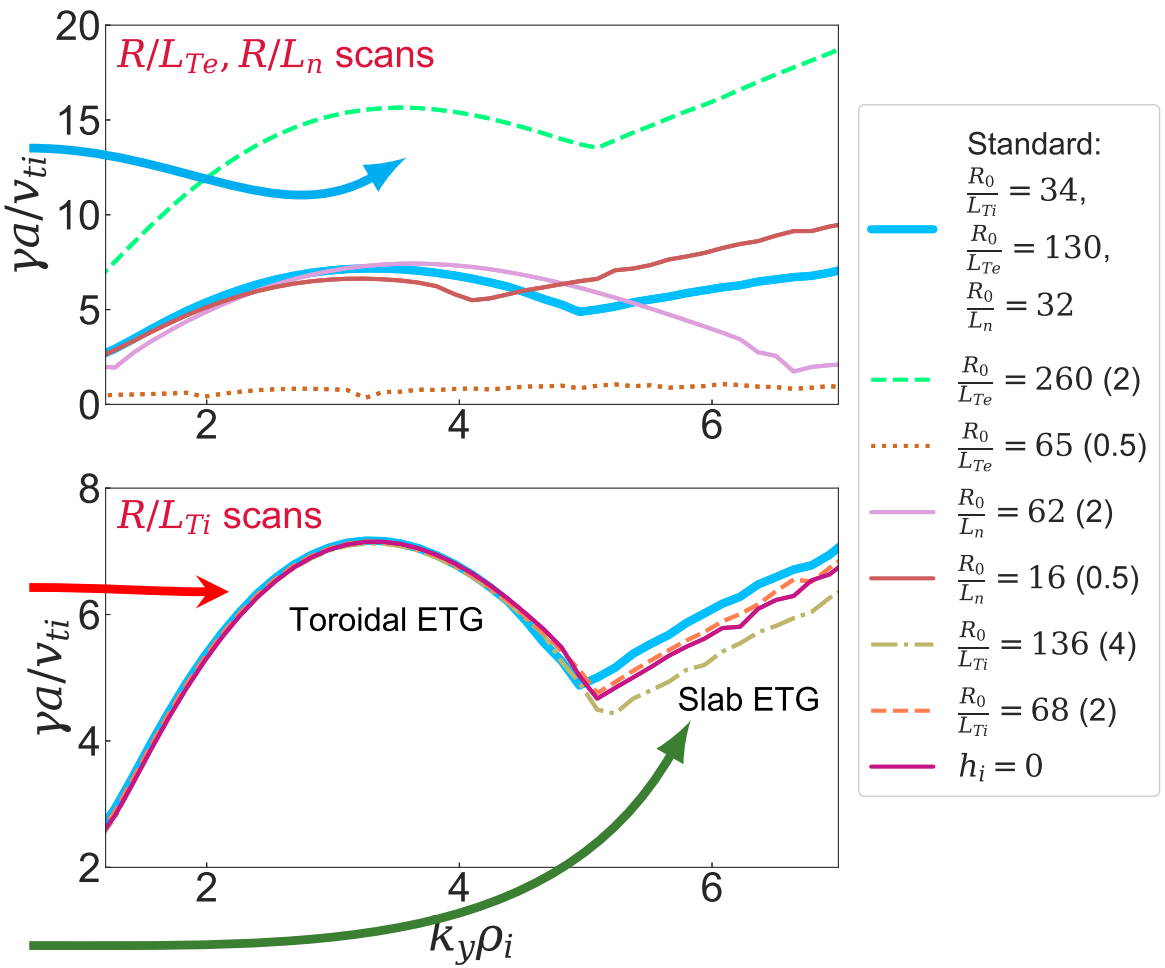

Figure 10: GS2 growth rate spectra for JET shot 92174.

Gyrokinetic Results ⟩ $1 \lesssim k_y\rho_i \lesssim 5$ Eigenmodes

Toroidal ETG eigenmodes localized at large θ.

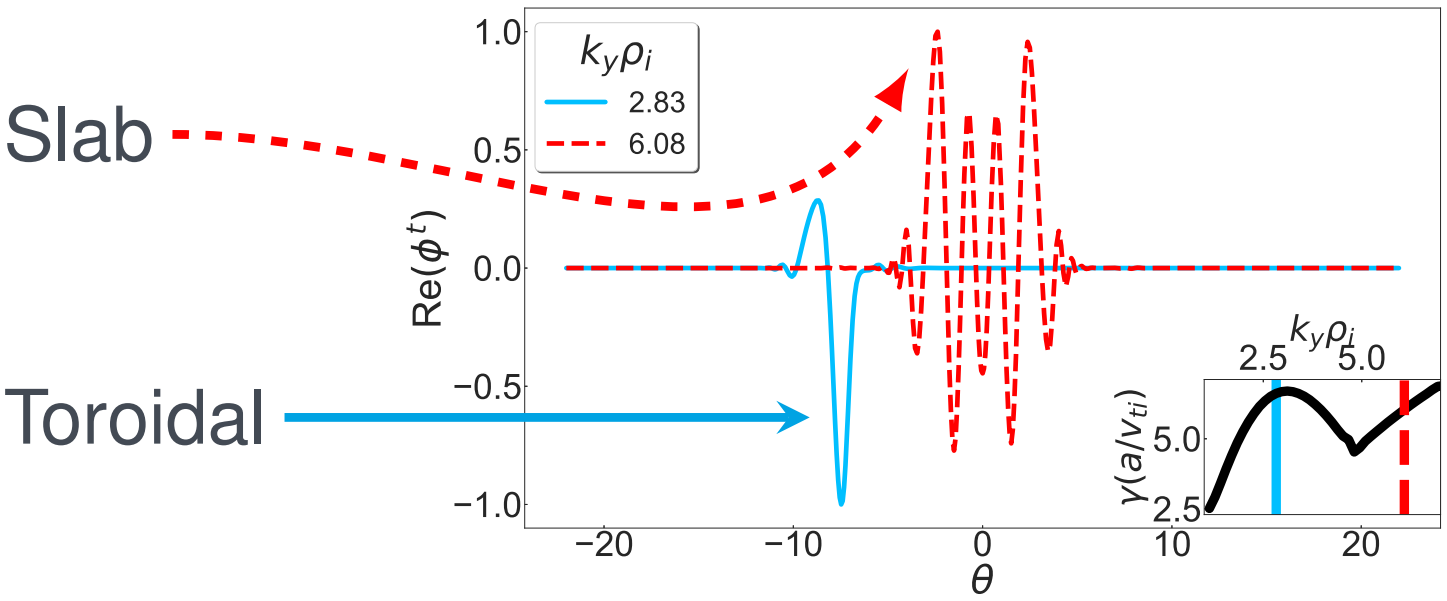

Figure 11: GS2 eigenmodes for toroidal (blue) and slab (red) ETG.

- In pedestal, toroidal ETG driven at $\hat{s}\theta \gg 1$ at $k_\perp\rho_e \sim 1$ with $k_x \gg k_y$ because $R/L_{Te} \gg 1$.
- Core ETG is ballooning in nature, peaking at $\theta = \theta_0 = 0$.
- Toroidal ETG eigenmodes in pedestal choose θ location based on combination of FLR effects and magnetic drifts ($\omega_{*e}\eta_e \sim \omega_{\kappa,e}$).

Toroidal modes driven only in bad curvature regions ($\omega_{*e}\eta_e\omega_{\kappa,e} > 0$).

- Flipping sign of $\omega_{\kappa,e}$ makes toroidal ETG mode jump to where $\omega_{*e}\eta_e\omega_{\kappa,e} > 0$.
- Good curvature $\Rightarrow$ roughly half of the θ domain is stable.

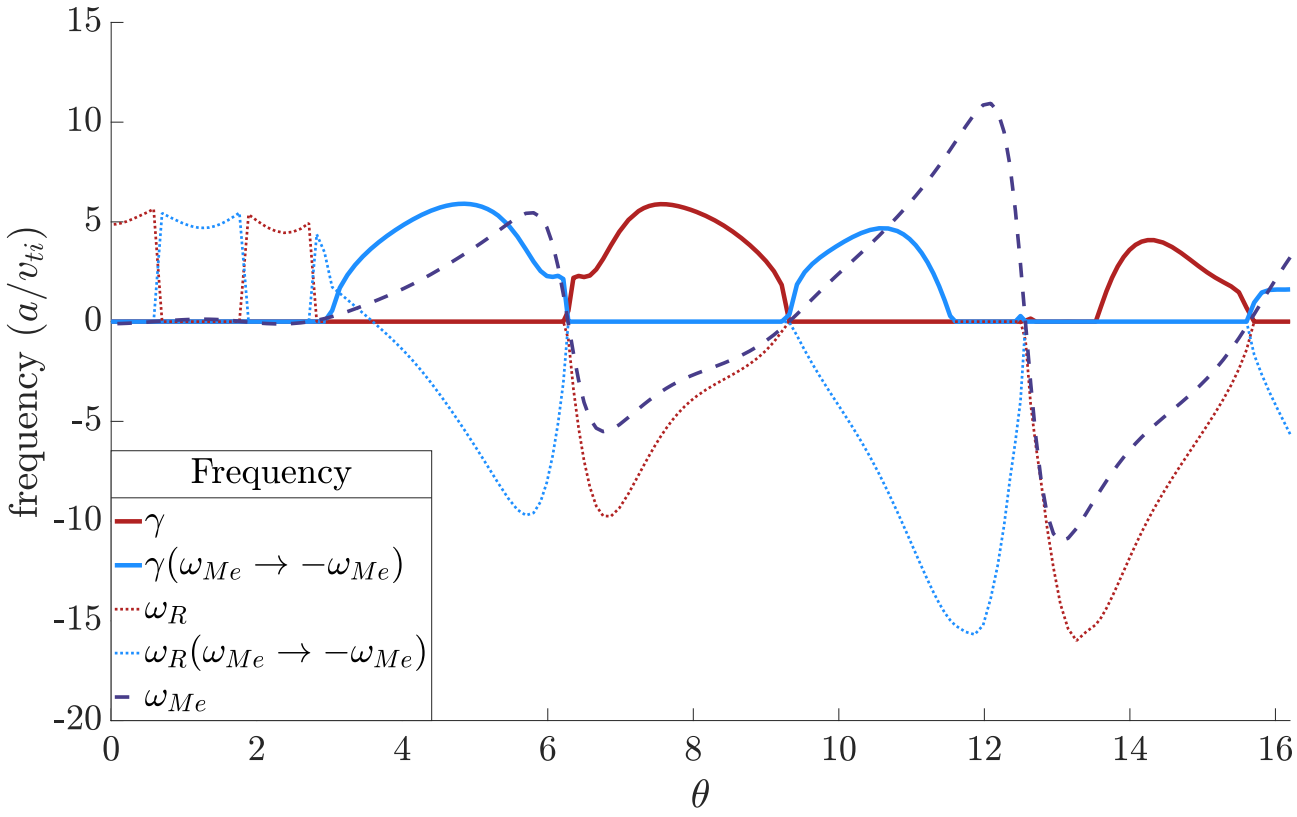

Figure 12: Linear growth rates versus θ for analytic dispersion relation, with $k_{\|} = 0$ and $\omega_{*e} < 0$. Flipping the sign of $\omega_{\kappa,e}$ changes the location where the mode can be driven.

FLR effects strongly determine the θ location for toroidal ETG.

- Mode has maximum amplitude very close to a local minimum in $k_\perp$, as shown below, where $\Gamma_0(b_e) = I_0(b_e)\exp(-b_e)$ and $b_e = (k_\perp \rho_e)^2/2$.
- Local minima in $k_\perp$ occur due to local magnetic shear.

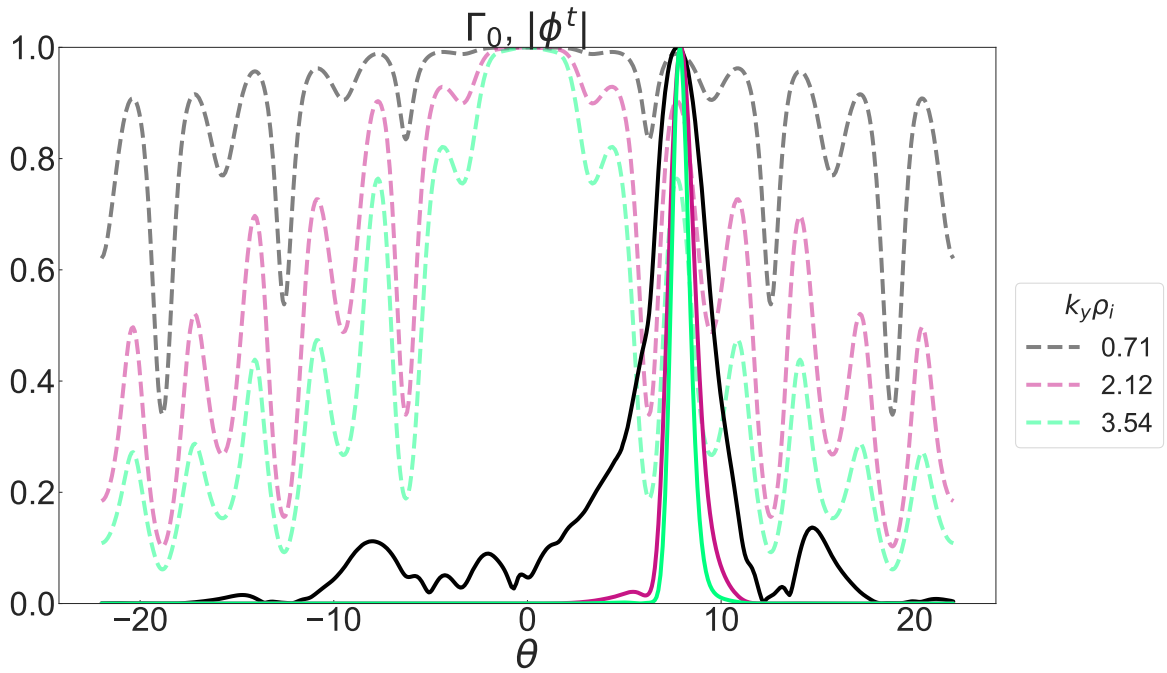

Figure 13: GS2 toroidal ETG eigenmodes (solid) and $\Gamma_0(b_e)$ for three separate k_y values.

Theory describes toroidal and slab ETG well.

- Local gyrokinetic dispersion relation describes toroidal and slab ETG surprisingly well.
- To find $k_{\|}$, we Fourier transformed GS2 eigenmodes.

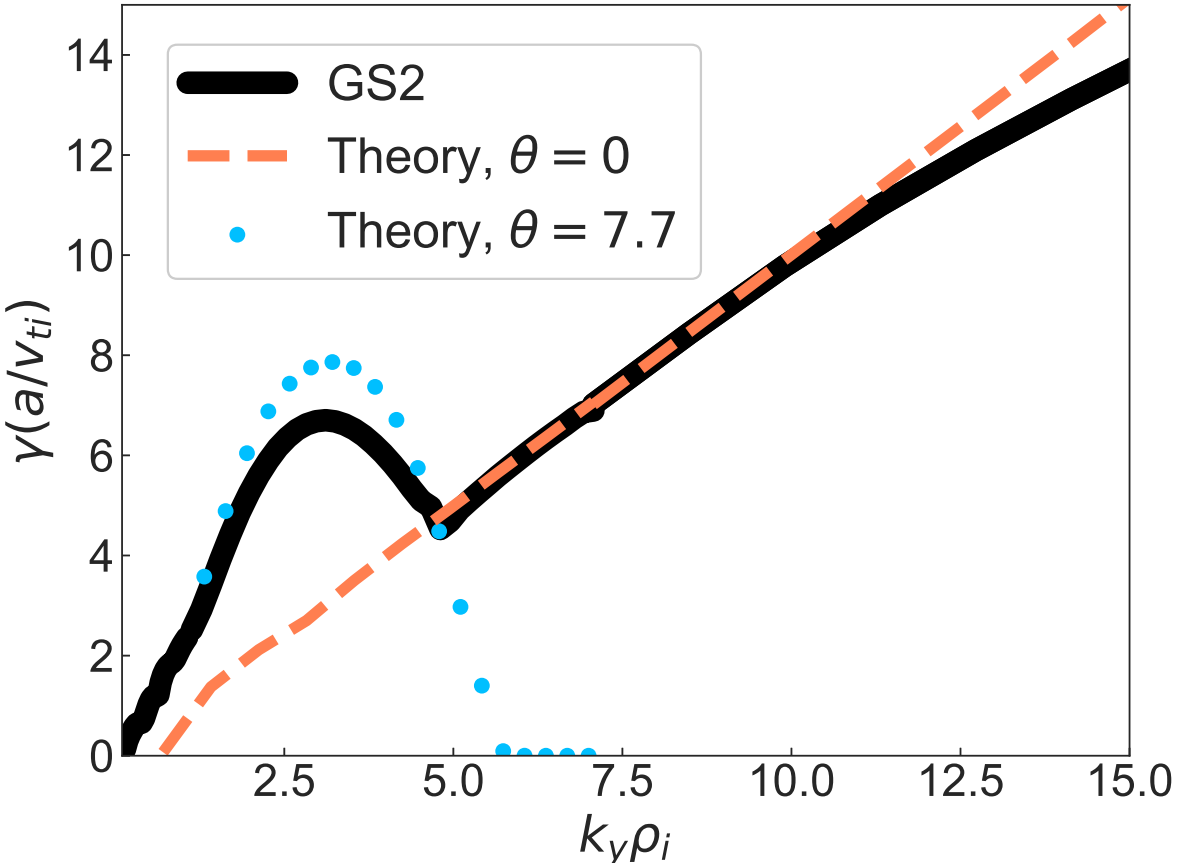

Figure 14: Linear growth rates from GS2 versus solutions to gyrokinetic dispersion relation.

Measured T_i profiles have subdominant ITG at almost all scales.

- We expect to drive strong slab and toroidal ITG at $k_y\rho_i \sim L_{Ti}/R \ll 1$.
- With the measured T_i profiles, ITG is almost completely suppressed at all scales.
- Regardless of ion gradients, electron temperature gradient driven modes dominate for $k_y\rho_i \gtrsim 0.2$

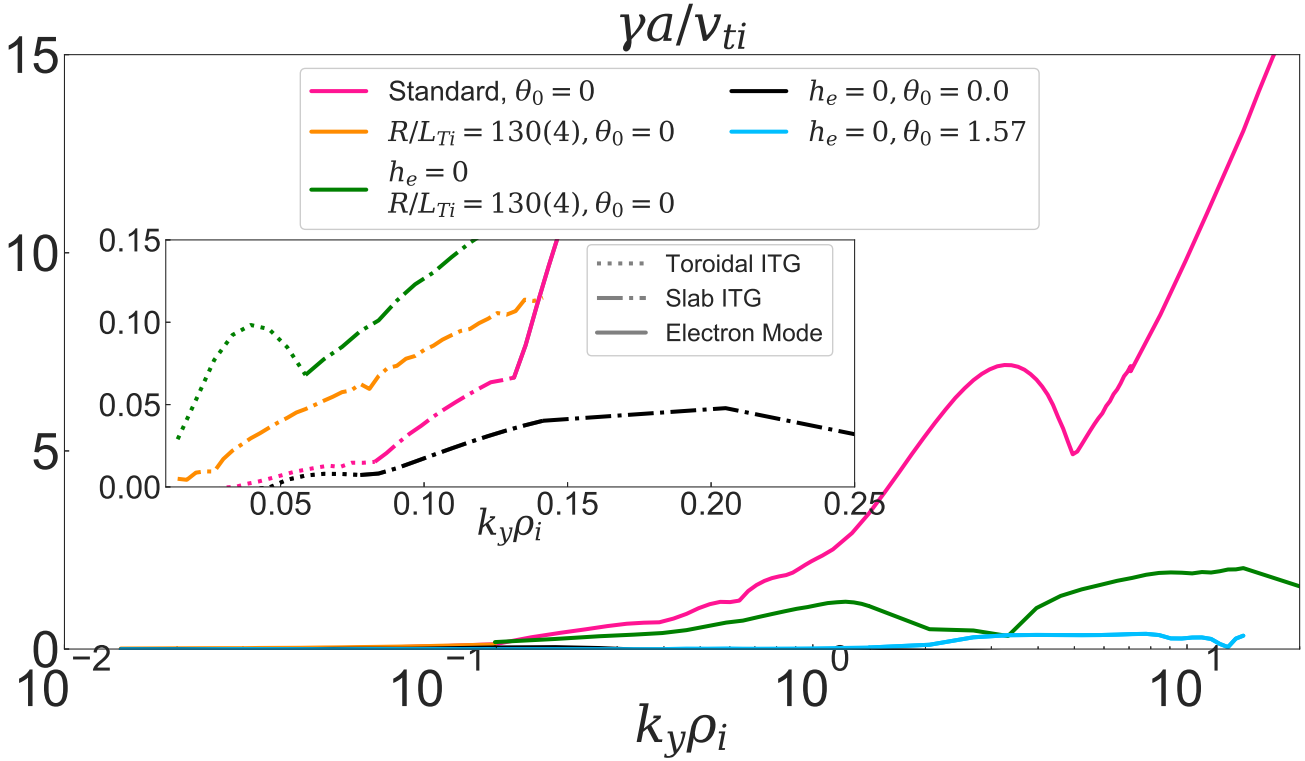

Figure 15: Full kinetic and adiabatic electron simulations with different R/L_{Ti}, shot 92174. The 'Standard' and '$h_e = 0$' cases differ by $h_e = 0$ and θ_0 values.

Summary 〉 Findings

- Toroidal ETG is driven at $k_y\rho_i \sim 1$ but $k_x\rho_e \sim 1$, because $R/L_{Te} \gg 1$.
- Slab ETG driven at scales as large as $k_y\rho_i \sim k_x\rho_i \sim 1$, because $R/L_{Te} \gg 1$.
- $\mathbf{E} \times \mathbf{B}$ shear suppresses KBMs, slab ITG in JET pedestals we investigated, toroidal ITG sometimes resilient, and ETG is not suppressed.
- Modes at almost all scales are most sensitive to electron temperature gradient physics.
- Local dispersion relation describes toroidal and slab ETG well.
- Even in the absence of flow shear, in shots we investigated, ITG is highly subdominant/absent because $\eta_i \sim 1$, R/L_{Ti} below critical value. **However**, ITG growth rate is extremely sensitive to measured T_i profile.

- Effects of θ_0 on linear toroidal ETG (*nearly solved*).
- Linear stability calculation for toroidal ETG with general $k_{\|}$ and full FLR effects (*nearly solved*).
- Effects of ions on slab ETG (*partly solved*).
- Nonlinear results (hard because multiscale, how important are these toroidal ETG modes?) (*unsolved*).
- Finding $k_{\|}$ self-consistently for toroidal modes (*unsolved*).
- Modes at $k_y \rho_i \lesssim 1$ (perhaps more transport relevant) (*unsolved*).

We gratefully acknowledge useful conversations with T. Adkins, J. R. Ball, N. Christen, M. R. Hardman, W. Guttenfelder, Y. Kawazura, J. C. Hillesheim, A. Mauriya, S. Saarelma, and A. A. Schekochihin. JFP is supported by EPSRC Scholarship No 3000207032. FIP, MB, and CMR are supported in part by the RCUK Energy-Programme (grant number EP/EPI501045). PGI is supported by an EU H2020 grant, agreement No 3000207035. Computational time provided by Plasma HEC Consortium EPSRC (grant number EP/L000237/1). This work has been carried out within the framework of the EUROfusion Consortium and has received funding from the Euratom research and training programme 2014-2018 and 2019-2020 under grant agreement No 633053 and from the RCUK Energy Programme [grant number EP/P012450/1]. The views and opinions expressed herein do not necessarily reflect those of the European Commission. The authors acknowledge EUROfusion, the EUROfusion High Performance Computer (Marconi-Fusion), the use of ARCHER through the Plasma HEC Consortium EPSRC grant numbers EP/L000237/1 and EP/R029148/1 under the projects e281-gs2, and software support from Joseph Parker through the Plasma-CCP Network under EPSRC grant number EP/M022463/1. JFP acknowledges travel support from Merton College, Oxford.

$$\mathbf{k}_\perp = k_x \nabla x + k_y \nabla y = \left[k_x - k_y\left(\hat{s}\theta - \frac{r}{q_c}\frac{\partial \nu}{\partial r}\right)\right]\nabla x \tag{8}$$

$$+ \frac{\partial \psi}{\partial r}\frac{1}{B_a} k_y \left[\nabla \zeta + \left(\frac{\partial \nu}{\partial \theta} - q\right)\nabla \theta\right], \tag{9}$$

using

$$\alpha = \zeta - q(x)\theta + \nu(x, y), \tag{10}$$

and the effective radial wavenumber is

$$k_x = k_{x0} - k_y\left(\hat{s}\theta - \frac{r}{q_c}\frac{\partial \nu}{\partial r}\right). \tag{11}$$

From quasineutrality, the electrostatic dispersion relation is,

$$Z_i \frac{T_{0e}}{T_{0i}} + 1 - \sum_s D_s = 0, \tag{12}$$

where

$$D_s = iZ_s^2 \frac{T_{0e} n_{0s}}{T_{0s} n_{0e}} \int_0^\infty d\lambda \frac{\Gamma_0(\hat{b}_s^\sigma)}{(1+i\sigma\lambda)^{1/2}(1+i\sigma\lambda/2)} \exp\left(i\lambda\widehat{\omega}\right) \exp\left(-\frac{(\lambda\widehat{k}_{\|})^2}{4(1+i\sigma\lambda)}\right)$$
$$\left[-\widehat{\omega} + \widehat{\omega}_{*s}\left(1 + \eta_s\left\{\frac{2(1+i\sigma\lambda) - (\widehat{k}_{\|}\lambda)^2}{4(1+i\sigma\lambda)^2}\right.\right.\right.$$
$$\left.\left.\left. + \frac{1}{(1+i\sigma\lambda/2)} - \hat{b}_s^\sigma \frac{1 - \Gamma_1(\hat{b}_s^\sigma)/\Gamma_0(\hat{b}_s^\sigma)}{(1+i\sigma\lambda/2)} - \frac{3}{2}\right\}\right)\right].$$

This is not a straightforward integral for $\gamma = 0$.

With

$$\frac{\mathbf{k}_\perp \cdot \mathbf{v}_{Mi}}{\omega} \sim \frac{(k_\parallel v_{ti})^2}{\omega^2}, \quad \omega \gg k_\parallel v_{ti}, \tag{13}$$

$$1 + \frac{ZT_e}{T_i}\left(1 - \frac{\omega_{*i}}{\omega} - \frac{\omega_{*i} k_\parallel^2 \eta_i T_i}{\omega^3 m_i} - \frac{\omega_{*i}\omega_{\kappa,i}\eta_i}{\omega^2}\right) = 0, \tag{14}$$

which for $k_\parallel = 0$, gives

$$\omega = 0, \quad \omega = \frac{\omega_{*i}}{2\left(1 + \frac{Z_i T_e}{T_i}\right)} \pm \sqrt{\frac{\omega_{*i}^2}{4\left(1 + \frac{Z_i T_e}{T_i}\right)^2} + \frac{\omega_{*i}\omega_{\kappa,i}\eta_i}{\left(1 + \frac{Z_i T_e}{T_i}\right)^2}}. \tag{15}$$

In GS2land, $\omega_{*e} < 0$.

With $R/L_n \gg 1$,

$$\gamma \sim \pm\eta_e \frac{\omega_\pm}{\omega_{*e}} \frac{R}{L_n}, \tag{16}$$

where

$$\omega_\pm = \pm\frac{\omega_{*e}}{2}\left(1 + \sqrt{1 - 8\frac{L_n}{R}\eta_i\frac{T_i}{T_e}}\right). \tag{17}$$

Eigenmodes Extended in θ.

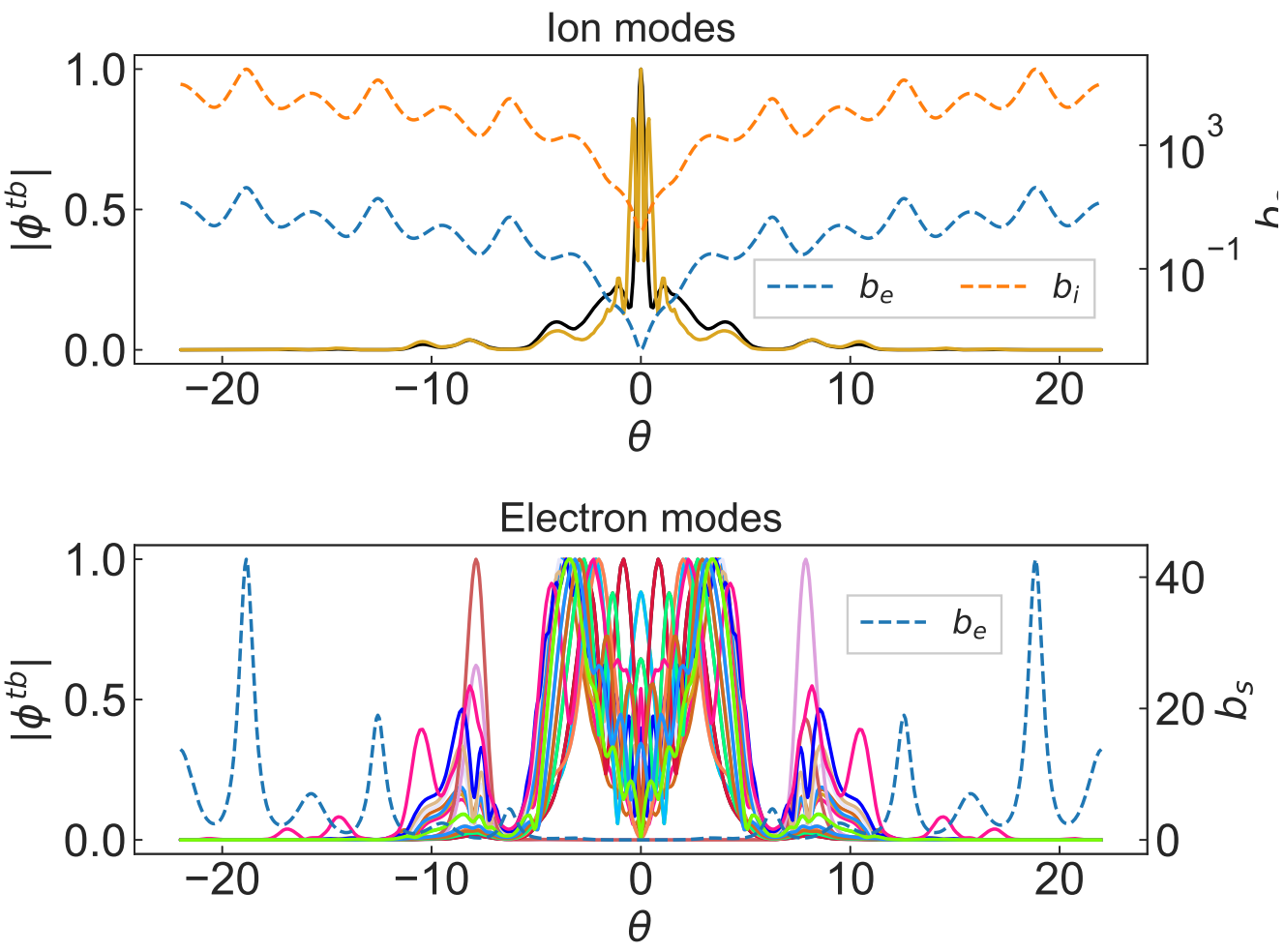

Figure 16: Electron and ion direction eigenmodes obtained using GS2 eigensolver at $k_y\rho_i = 3.5$.

ITG has very low growth rates in our pedestals.

- Using GS2 eigensolver mode, we find a single very weak ITG-like mode at $k_y\rho_i = 3.5$, from two modes in the ω_{*i} direction.
- For this ITG mode, $\gamma a/v_{ti} = 0.07$, whereas for the fastest growing ETG mode at $k_y\rho_i = 3.5$ has $\gamma a/v_{ti} = 7.1$.

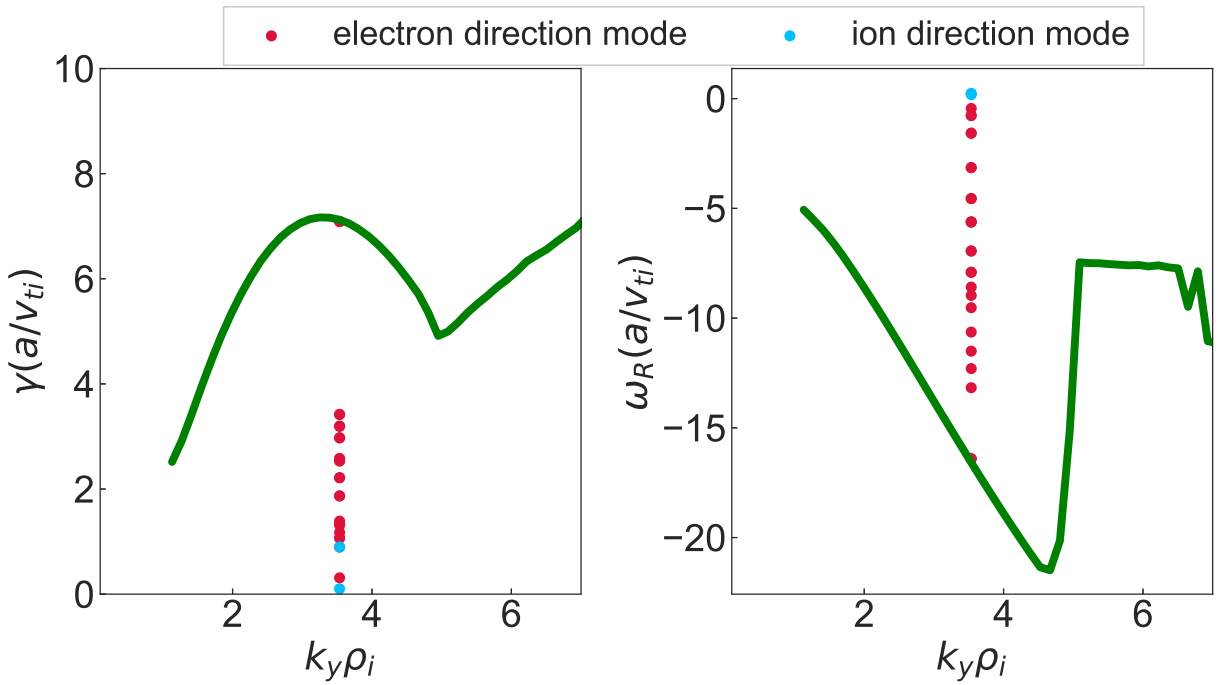

Figure 17: Imaginary (left) and real (right) frequencies for the 17 eigenmodes found at $k_y\rho_i = 3.5$.

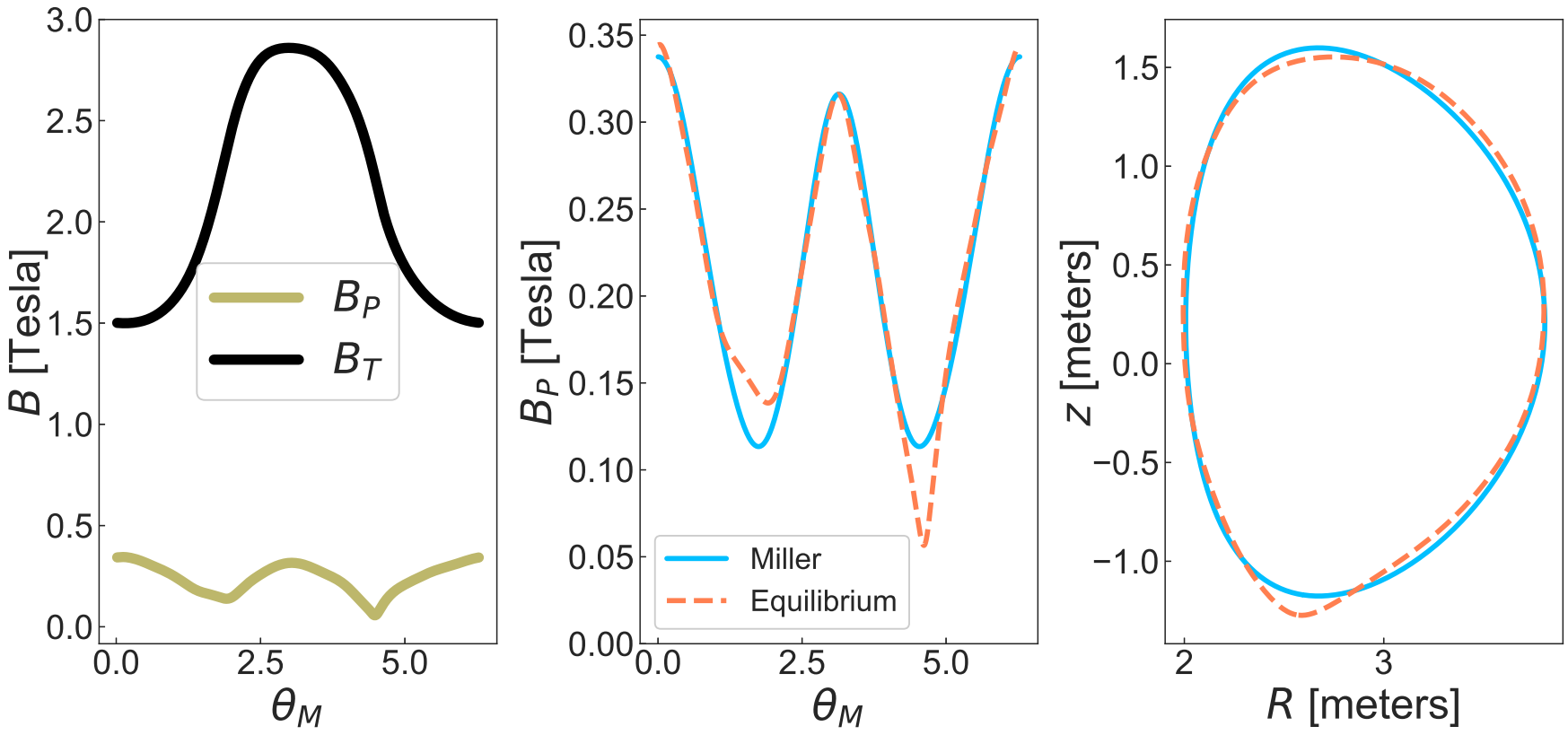

Figure 18: Miller equilibrium for JET shot 92174.

Equilibrium pedestal profiles are very steep in the pedestal.

⇒ expect microinstabilities to be strongly driven.

- Measured T_i flatter than T_e in pedestal.
- Pedestal electron measurements in 80-99% ELM interval from HRTS, ion measurements in 60-99% ELM interval from CXRS.
- Investigated implications of $T_i = T_e$, $T_i \neq T_e$, equal and different gradients.

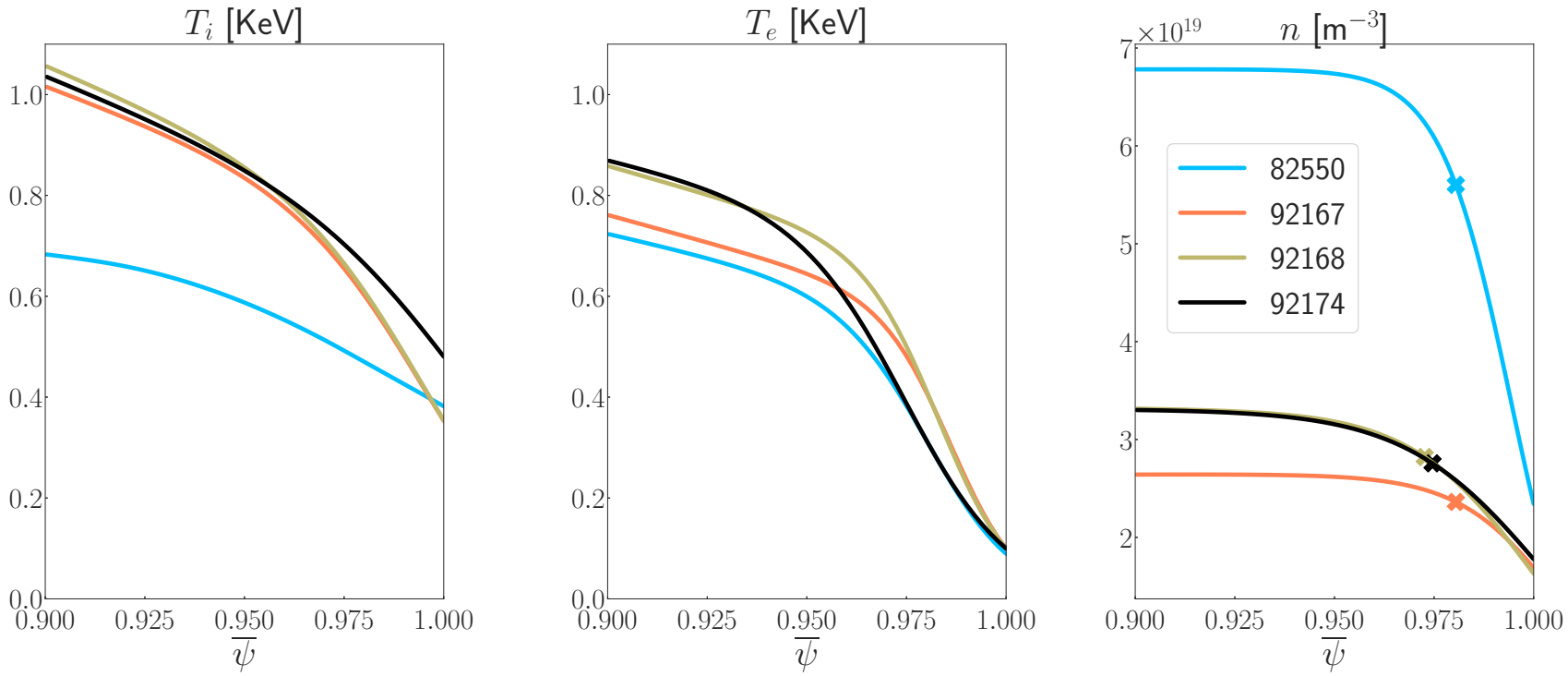

(a) Ion temperature (b) Electron temperature (c) Density

Equilibrium gradients are much bigger than in the core.

- $R/L_{Te} \approx 50 - 400$, $R/L_{Ti} \approx 30 - 100$. In core, $R/L_{Ts} \approx 5 - 10$. Here R is the major radius, $L_{Ts} \equiv |\nabla \ln T_s|^{-1}$.

  $\Rightarrow$ dramatic consequences for ITG and ETG stability!

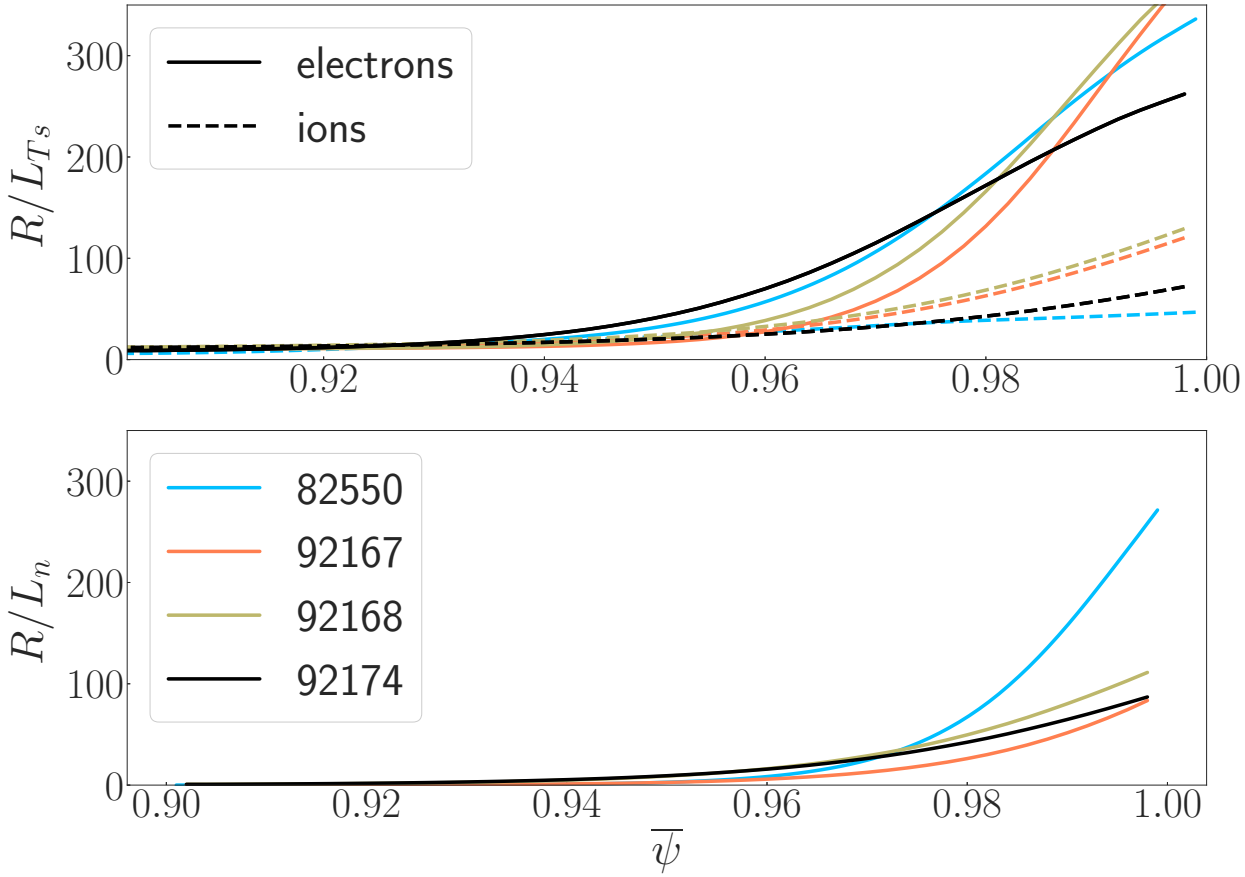

Figure 20: Temperature and density gradients

Linear spectra at wide range of scales.

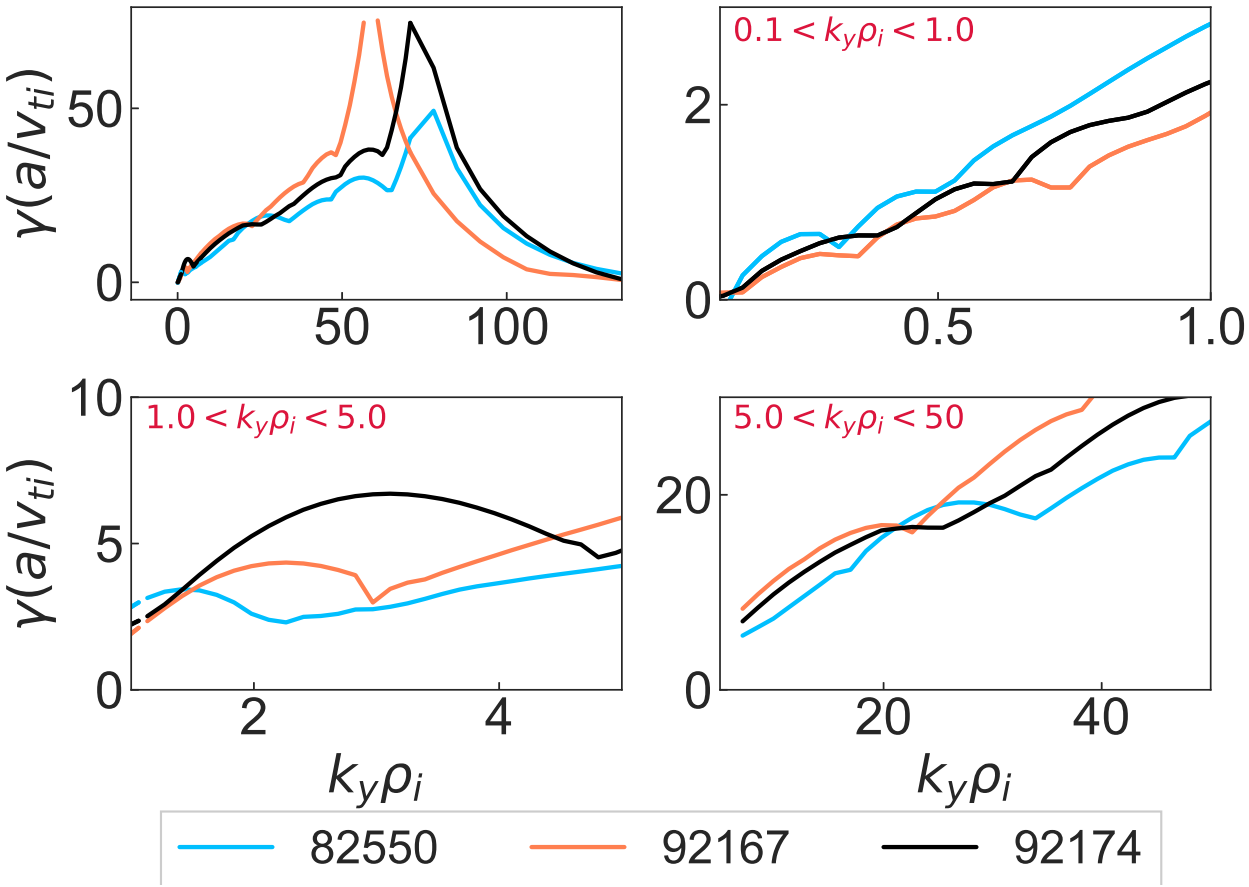

Figure 21:

Linear spectra.